JTTEE5 19:531–540
DOI: 10.1007/s11666-009-9412-4
1059-9630/$19.00 © ASM International

Temperature-Dependent Properties of Spray-Deposited ITO Thin Films

A.V. Moholkar, S.M. Pawar, K.Y. Rajpure, P.S. Patil, C.H. Bhosale, and J.H. Kim

(Submitted January 17, 2009; in revised form July 16, 2009)

Sprayed indium tin oxide (ITO) thin films are synthesized by mixing adequate quantities of ethanolic solutions of indium trichloride and stannic chloride at different substrate temperatures. The pyrolytic decomposition temperature affects the properties and morphology of ITO samples. X-ray diffraction results showed that the films are polycrystalline with cubic structure and exhibit preferential orientation along (222) plane. The SEM and AFM studies indicated that the surface morphology of the samples increases with substrate temperature. The typical I_{500} sample is composed of cubic grains and has carrier concentration of 3.26×10^{20} cm^{-3} and mobility of 9.77 cm^2/V s. The electrical resistivity of ITO films decreased with increasing deposition temperature. The highest figure of merit of film is 4.4×10^{-3} Ω^{-1}. Optical absorption studies reveal that films are highly transparent in the visible region and band gap increases with substrate temperature owing to Moss-Burstein effect.

Keywords atomic force microscopy, oxides, semiconducting materials, x-ray diffraction

1. Introduction

Recent optoelectronic applications require improvements in the physical and chemical properties of transparent conducting oxides (TCOs) thin films. Among different TCOs, namely SnO_2:F (FTO), SnO_2:Sb (ATO), ZnO:Al (AZO), ZnO:Ga (GZO), In_2O_3:Sn (ITO) has the unique characteristics such as highest electrical conductivity, high optical transmittance over the visible wavelength region, and excellent adhesion to the substrates. These films are used in a number of applications, namely flat-screen high-definition televisions, high-resolution screens on portable computers, electrochromic windows, handheld new smart displays, optoelectronics, flat panel displays, solar cells, gas sensors, photo-catalysts, photo-electric-catalysis, etc. (Ref 1-3). TCO films can be n- or p-type semiconductor depending upon incorporated donor impurity (Ref 4, 5). The influence of microstructure and composition on the electrical and optical properties of ITO thin films is reported (Ref 6). Various deposition techniques have been widely used to produce ITO thin films. However, seeking the most reliable and economic deposition technique is the main goal. The most intensively studied techniques are spray pyrolysis (Ref 7-16), sol-gel process (Ref 17), RF sputtering (Ref 18), evaporation (Ref 19), magnetron sputtering (Ref 20), electron beam evaporation (Ref 21), and pulsed laser deposition (Ref 22). The spray pyrolysis is one of the simplest deposition techniques because of its simplicity and it provides large area coatings without high vacuum ambience. So the capital cost and the production cost of high quality metal oxide thin films are expected to be the lowest among all the thin film deposition techniques. Furthermore, this technique is also compatible with mass production system. Also, the coatings produced with the spray pyrolysis are inherently uniform and the surface-to-volume ratio of the nano drops are very large making them very receptive to heat treatment and pyrolysis. Further, relatively moderate temperature heat treatment is only necessary for the growth of highly oriented thin films on different semiconductor substrates for device applications (Ref 23).

In spite of enormous literature on synthesis and characterization of ITO thin films by different methods, the attempts are still going on to improve their properties especially the figure of merit, which requires high conductivity and high optical transmittance. This study focuses on optical, structural, morphological, and electrical properties of sprayed ITO thin films, prepared particularly, to achieve highest figure of merit using lower precursor quantity.

2. Experimental

The chemical spray pyrolysis technique (SPT) is one of the major techniques to deposit a wide variety of thin films. It can use a variety of atomization techniques such as ultrasonic nebulizer, spray hydrolysis, corona spray pyrolysis, electrostatic spray pyrolysis, etc. (Ref 24). The soda lime glass substrates of size ($25.4 \times 75 \times 1.2$ mm^3)

A.V. Moholkar, Department of Physics, Gopal Krishna Gokhale College, Kolhapur 416 012, MS, India; **A.V. Moholkar, S.M. Pawar,** and **J.H. Kim**, Department of Materials Science and Engineering, Chonnam National University, 300 Yongbong-Dong, Puk-Gu, Gwangju 500-757, South Korea; and **K.Y. Rajpure, P.S. Patil,** and **C.H. Bhosale**, Electrochemical Materials Laboratory, Department of Physics, Shivaji University, Kolhapur 416004, MS, India. Contact e-mail: avmoholkar@yahoo.co.in.

supplied by Blue Star, Mumbai, were initially boiled in chromic acid for 10 min, washed with double distilled water and dipped in labolene detergent and again washed with double distilled water. The substrates were further ultrasonically cleaned for 15 min, prior to the deposition. The different types of atomizers, such as air blast, pneumatic, ultrasonic, and electrostatic, are being used for the thin film deposition (Ref 24). These atomizers differ in droplet sizes which again depend on the solution density, viscosity, and surface tension. In this study, specially designed nozzles were used. Further the quality of the deposits depends on capillary diameter and shape of the nozzles like saw-tooth, wedge, and flat tips. The better uniformity and dense coating is achieved with flat tip nozzle (Ref 12) and therefore the different flat tip homemade nozzles from borocil glass tubes were made and tested. The best one with outer and inner diameters of 5 and 0.2 mm, respectively, gives optimistic yield. The solution passes through the inner capillary tube surrounded by gas tube through which carrier gas flows. Due to this, a vacuum is created at the tip to suck the solution from the tube and then spray starts. The substrate is kept stationary; while to and fro motion of nozzle is achieved using an electrical stepper motor. The optimization of the process parameters is a prerequisite, and several trial experiments were carried out to optimize. Initially, the ITO films were deposited by keeping the substrate temperature constant in order to optimize spray rate, nozzle to substrate distance, carrier gas pressure. After each set of deposition, the transmittance and the resistivity of the films were measured, and then their figure of merit was estimated. The parameters corresponding to maximum figure of merit were considered as optimized one. The optimized values of important parameters are air flow rate (1.5 kg/cm^2), spray rate (5 mL/min), distance between substrate to nozzle (28 cm), solution composition (25 mM), tin doping (5 wt.%), and quantity of the spraying solution (50 mL). The influence of these parameters on the ITO films has been reported elsewhere (Ref 8, 9). Thereafter, ITO thin films were prepared by spraying an ethanolic solution containing indium chloride and stannic chloride at different substrate temperatures ranging from 450 to 525 °C at an interval of 25 °C. Compressed air was used as a carrier gas. The gas regulator valve is used to control the pressure of the carrier gas flowing through the gas tube of the spray nozzle. A corning glass tube of length 25 cm and of diameter 1.5 cm is converted into gas flow meter. The iron disc, with diameter 16 cm and thickness 0.7 cm, was supported on the electric heater (2000 W). Maximum temperature up to 600 °C can be obtained with this arrangement. The substrates were positioned horizontally on the heating plate, which was placed over the heater. Chromel-alumel thermocouple was used to measure the temperature of the substrates and is fixed at the center of the iron disc. The temperature of the hot plate was monitored with temperature controller model, 9601 (Aplab make). Hazardous fumes were expelled out from deposition chamber using an exhaust system attached to the spray pyrolysis unit. After the deposition, the heater was switched off and these films were allowed to cool at the room temperature. All the films were transparent, well adherent, and pinhole free and were further used for optical, electrical, and structural characterization.

Using Systronics make UV-Vis Spectrophotometer (Model 119), the transmittance of the films was recorded at normal incidence in the 200-850 nm spectral range. Since absorption was measured for the film deposited on glass substrate, it was necessary to measure the absorption by the bare glass plate prior to the deposition of ITO film. This spectrum was subtracted from the spectrum obtained with ITO film deposited over the glass substrates to get the actual transmission of ITO film. The thickness of ITO thin films was determined by etching away the part of the films. The 6 M HCl + 0.2 M $FeCl_3$ was used as etchant (Ref 25) in which the samples were placed vertically. After etching, the samples were rinsed in deionised water, the resist stripped in acetone and AMBIOS-XP-1 surface profiler was used to measure the step. The thickness of samples was divided by the time (in seconds) required for spraying the total quantity of the solution and is termed as the growth rate. The structural properties were studied by Philips x-ray diffractometer model PW-1710 using Cu K_α (1.5418 Å) radiation. The microstructure of the ITO films was studied by SEM (JEOL JSM 6063) and atomic force microscopy (AFM) using contact mode with Si tips at a scan rate of 1 Hz, using Veeco, CP II, scanning probe microscope. The electrical measurements like resistivity (ρ), sheet resistance (R_s), carrier concentration (n), and mobility (μ) were carried out at room temperature by using Hall effect setup supplied by Scientific Equipments, Roorkee, India in Van der Pauw configuration.

3. Results and Discussion

The ITO thin films were synthesized over fixed range of substrate temperature (450-525 °C). Below 450 °C, films are not formed since it is not enough temperature to complete the chemical reaction, wherein the droplet hit on the substrate removing a lot of heat leading to a partial decomposition of starting materials. The enhancement of film properties, deposited above 450 °C is due to the growth of the films carried at low temperature CVD process, in which the solvent vaporizes near to the surface substrate then the resulting solid melts and vaporizes and vapor diffuses to the substrate (Ref 26). Preliminary experiments showed inferior quality of thin films below 450 °C, and glass substrates get deformed above 525 °C. Hence this study includes the data of the ITO films synthesized within this temperature range. The samples deposited with different substrate temperatures are denoted as I_{450}, I_{475}, I_{500}, and I_{525}.

3.1 Transmittance and Thickness Measurements

Figure 1 shows the thickness variation of ITO films with substrate temperature. It varies over 250-440 nm. The films deposited at substrate temperatures $<$450 °C are milky and not adherent, whereas uniform and transparent films are formed above 450 °C substrate

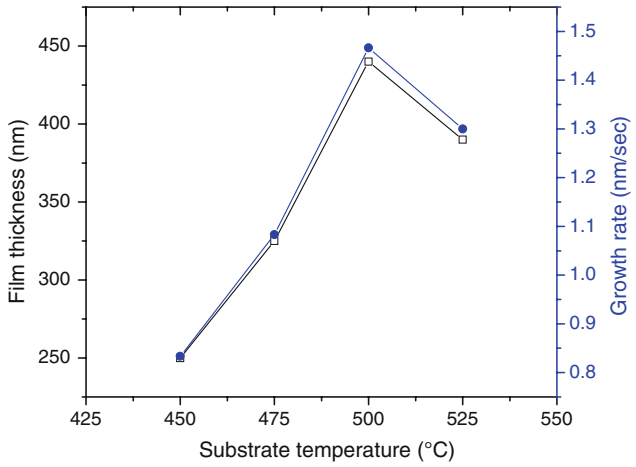

Fig. 1 Variation of film thickness and growth rate of the ITO thin films as a function of substrate temperature

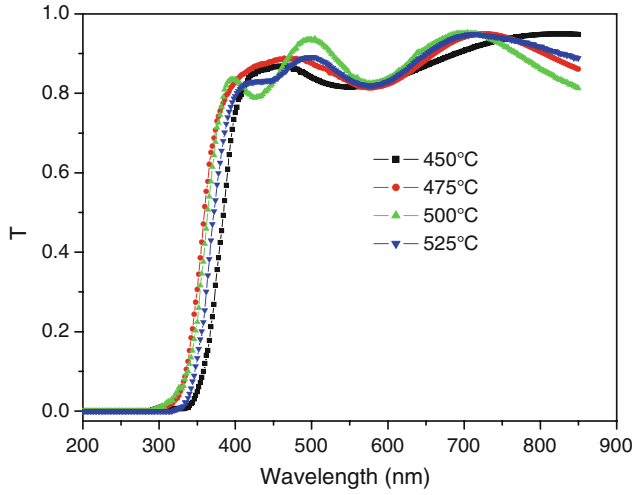

Fig. 2 Variation of transmittance of the ITO thin films deposited at different substrate temperatures

temperature. Figure 1 shows that the growth rate increases from 0.83 to 1.46 nm/s for I_{450} to I_{500} samples and then decreases to 1.3 nm/s for I_{525} sample. This can be explained as follows: low substrate temperatures, e.g., 450 °C, may not be sufficient to decompose the sprayed droplets containing Sn^{4+} and In^{3+} ions completely and un-reacted precursor is swept away by subsequent droplets reaching well before the surface, resulting in a low growth rate. On the other hand, the decrease in growth rate for I_{525} sample is due to a higher evaporation rate of the solvent (Ref 3, 23, 26, 27), leading to premature drying up of a part of the spray droplets before reaching the substrate. The occurrence of an optimized temperature leading to maximum growth rate for tin oxide thin films has been reported (Ref 28).

3.2 Optical Absorption Studies

Optical characterization of thin films gives information about physical properties, like band gap energy, band structure and optically active defects, etc. The transmittance values for ITO samples include the contributions from the glass substrate and the coated films. The samples at lower substrate temperature exhibited a dark milky appearance due to the low wavelength absorption at a low-temperature deposition. Figure 2 shows the optical transmittance curves as a function of wavelength of the studied ITO films. The optical transmission falls very sharply near the UV region due to the onset of fundamental absorption. The optical properties of the I_{450} to I_{525} sample do not change significantly, and all the samples are highly transparent (>85% at 550 nm). The higher transmittance observed in the films is attributed to less scattering effects, structural homogeneity, and better crystallinity, whereas, the lower transmittance in the layers grown at temperatures <450 °C might be due to the less crystallinity leading to more light scattering (Ref 15, 17, 29). On the other hand, the oscillation of the transmittance curve is attributed to the interference of the light refracted from the surface of the thin film. Further, the fundamental

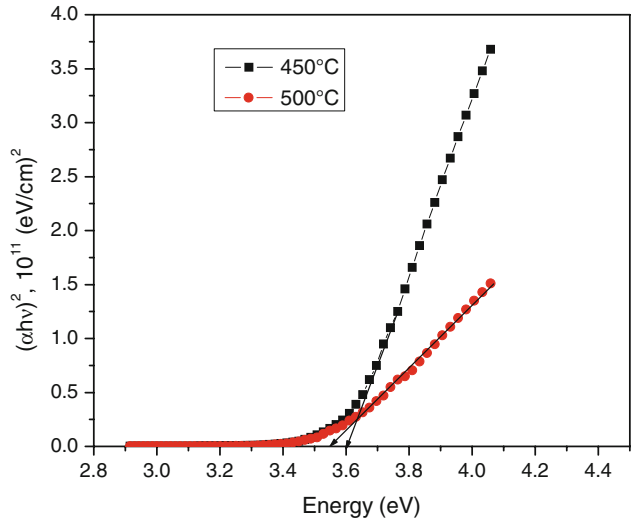

Fig. 3 The typical plots of $(\alpha h\nu)^2$ vs. $h\nu$ for ITO thin films deposited at 450 and 500 °C

absorption edge was shifted toward shorter wavelengths with the increase of deposition temperature. Thus, the combined effect results in the transmission of the wider range of the solar spectrum. The conductivity of the material is also observed to be increasing. Thus, a correlation between the shifting of the absorption and the increase in the electrical conductivity due to the increase in carrier density is expected.

For the direct transition, the optical band gap energy of ITO film is determined using the equation $\alpha h\nu = A(h\nu - E_g)^{1/2}$, where "$h\nu$" is the photon energy and "E_g" is the optical band gap and A is a constant. The typical plots of $(\alpha h\nu)^2$ versus $h\nu$ for I_{450} and I_{500} samples are shown in Fig. 3. The optical band gap energy "E_g" value of these samples increases from 3.56 to 3.74 eV. In most cases, the films present a sharp absorption edge

at wavelengths of about 320-350 nm. Concerning the effect of the change of deposition temperature, a slight decrease of reflectivity associated with the absorption edge is observed, indicating an increase of the optical band gap. It is reported that the absorption edge shifts toward shorter wavelength, suggesting a widening of energy band gap with increasing substrate temperature. The direct gap is determined by extrapolating the linear portion of $(\alpha h\nu)^2$ to the energy axis to $\alpha = 0$. The optical band gaps, thus determined are not the actual band gaps of the material. Since these are degenerate semiconductors, the Fermi level lies within the conduction band where its position depends on the density of the free electrons. Thus, the values given for the optical band gaps are related to the excitation of the electrons from the valance band to the Fermi level in the conduction band, whereas the actual band gap of the material is related to the excitation of the electrons from the top of the valence band to the bottom of the conduction band. The increase of the optical band gap energy with deposition temperature is attributed to the so-called Moss-Burstein effect (Ref 11, 15, 30-32). The fact that the onset of light absorption is shifted toward lower wavelengths in thin films, especially highly doped ones, turns out to be an advantage for optical applications in the UV.

3.3 X-ray Diffraction Analysis

The substrate temperature (>450 °C) is not sufficient to attain the reaction rate required for perfect decomposition of the ingredients and films with foggy nature are formed. For I_{500} sample, a sustained thermal reaction is taking place in which the film formation mechanism is associated with the volatization of the precipitated indium salt and diffusion of the resulting vapor to the heated substrate, followed by its decomposition to the ITO films. The substrate temperature above 525 °C leads to a homogeneous nucleation of the vapor phase forming oxide particles and clusters of particles on the substrate due to which the films with nonuniform surface are observed. Figure 4 shows x-ray diffraction analysis (XRD) spectra of I_{450}, I_{475}, I_{500}, and I_{525} samples. The calculated "*d*" values (Table 1) are in good agreement with the standard "*d*" values of ASTM card 16-1665. Body centered cubic structure with the (222) predominant plane of crystallization has been identified for all the samples. Other planes (211), (400), (440), and (622) are also observed with small intensities. The graph of relative intensities of two major peaks such as (200) and (400) of the deposited ITO films as a function of substrate temperature is plotted in Fig. 5. It is seen that with rise in substrate temperature this ratio increases and is maximum for I_{500} sample and thereafter it decreases. The peak intensity and number of peaks increase with increase in the substrate temperature and are attributed to the improved crystallinity of ITO thin films. The ratio is strongly correlated to the sheet resistance of the ITO; although it is unknown whether this is a cause-and-effect relation. This strong correlation reflected the fact that the sheet resistance of the ITO is reduced (Fig. 10) and the intensity ratio of the (222) peak to (400) peak increased, as the deposition

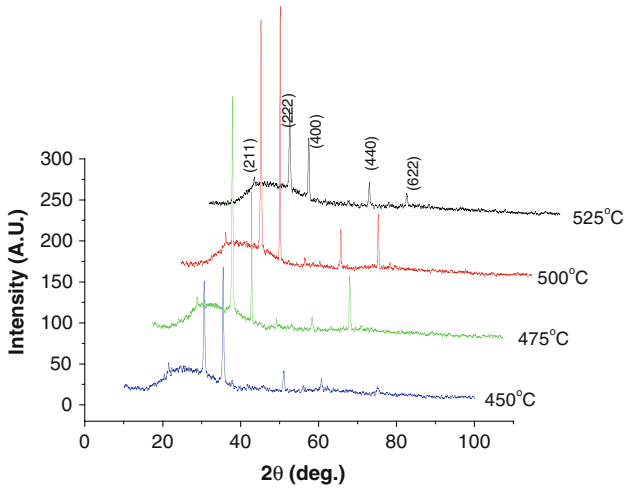

Fig. 4 XRD spectra of ITO films deposited at different substrate temperatures

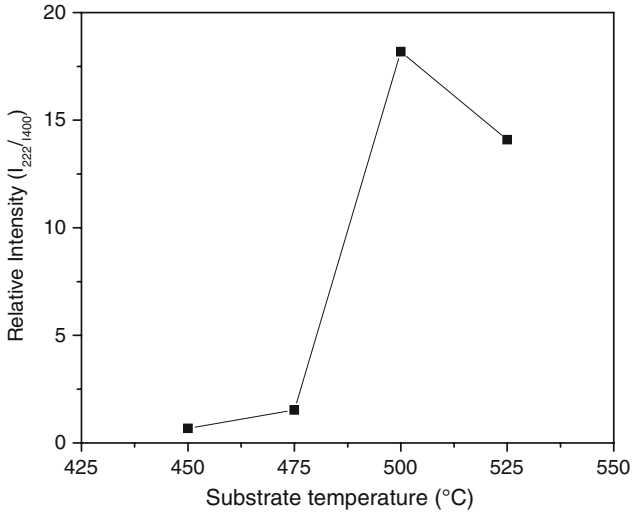

Fig. 5 The plot of ratio of relative intensity of 222/400 planes as a function of temperature

Table 1 Comparison of observed "*d*" values with standard "*d*" values for ITO thin films deposited at different substrate temperatures

		Observed *d* (Å) values for ITO samples			
(*hkl*)	Standard *d* (Å)	I_{450}	I_{475}	I_{500}	I_{525}
211	4.13	···	4.0744	4.1325	4.1487
222	2.921	2.915	2.921	2.9219	2.9159
400	2.529	2.5239	2.5311	2.5332	2.528
411	2.385	2.3765	···	···	···
332	2.157	···	2.1548	2.1573	···
431	1.984	1.9844	1.9803	···	···
440	1.788	1.7874	1.7881	1.7871	1.7876
622	1.525	1.5236	1.5255	1.5264	1.5255
444	1.46	···	1.4598	1.4597	···
761	1.0911	···	···	1.0896	···

temperature increased. A change in the preferred orientation between (400) and (222) has been also reported (Ref 14). The mean crystallite size (D) calculated for (222) plane using standard Scherer's formula (Ref 33) varies from 45 to 66 nm for I_{450} to I_{500} samples and is 62 nm for I_{525} sample. At higher temperature, the crystallites seem to be smaller, which may probably due to the re-evaporation of the film.

3.4 Morphological Studies

In spray pyrolysis except for aerosol generation, the deposition temperature is involved in many processes, such as aerosol transport, solvent evaporation, droplet impact with consecutive spreading, and precursor decomposition. It can change a cracked morphology into porous microstructure and properties of the films, in turn (Ref 27). The spray process involves different steps such as (1) solution is converted into small aerosols like droplets; the droplet size (x) and number of droplets formed per unit time per unit area of cross section (y) depends on nozzle geometry, carrier gas flow, and solution flow rates. We presume that x and y remain unchanged, as all the parameters are fixed and only substrate temperature is varied; (2) sprayed droplets move toward hot substrates kept at the bottom of the reactor with velocity (z); (3) droplets undergo pyrolytic decomposition; the degree of decomposition depends on the substrate temperature and temperature gradient formed near the substrate. As substrate temperature is varied in the present investigation; and (4) small grains are formed on the substrate; the grains may grow individually or get agglomerated depending on their surface mobility, which primarily depends on surface temperature. Hence the properties and morphology changes with deposition temperature, and such type of nature is reported by others as well (Ref 10, 11, 13, 14, 23, 26).

3.4.1 SEM Studies. Figure 6 shows the SEM micrographs of I_{450}, I_{475}, I_{500}, and I_{525} samples. The surface morphology of the I_{450} sample reveals nanosized grains emerging from the solute deposited on to the substrate. The cloudy splashes of the solute formed due to impingement of the sprayed droplets are seen in the background. This is a premature growth of grains owing to incomplete "P_d" of the sprayed solution at lower (in the studied range) substrate temperature (450 °C).

The cloudy background disappears as pyrolytic decomposition "P_d" increases and nanosized grains become clearly visible for the sample I_{500}. Few grains get agglomerated due to limited surface mobility "S_m" and form small-sized rope-like structures. Upon further rise in substrate temperature, i.e., for I_{525} sample, "S_m" plays a pivotal role and due to high S_m, most of the grains agglomerate to form compact structure of larger sized grains. For highest studied substrate temperature, I_{525} sample, "P_d" is very large and droplets are converted in to vapor that diminish mass deposited on to the substrate. This causes decrease in film thickness and random distribution of uneven grains. The effect of surface mobility on the nucleation and island growth of ITO thin films has been reported by Xu and Lu (Ref 34).

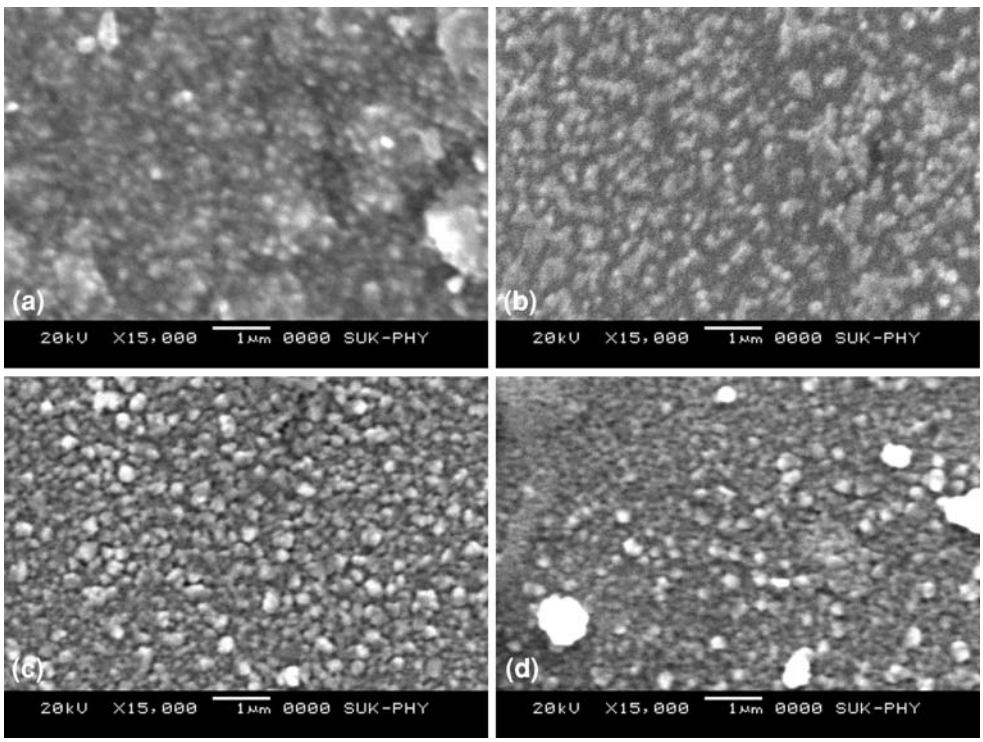

Fig. 6 SEM images of the ITO films deposited at substrate temperature of (a) 450 °C, (b) 475 °C, (c) 500 °C, and (d) 525 °C, respectively

3.4.2 AFM Studies. The film microstructure reflects unidirectional transfer of atoms from the gas phase to a substrate and this is greater in sputtering and evaporation than in CVD processes. Shadowing effects, substrate temperature, and energy of the depositing atoms are the influencing factors that affect grain morphology. At elevated temperature, both surface and bulk diffusion allow atoms to access equilibrium lattice sites, fill voids, and enlarge grains (Ref 35). The growth mechanism of the ITO films at high substrate temperature with an interesting transition from a 3D island growth mode at low temperatures to 2D growth at higher temperature is reported (Ref 36, 37). Kim et al. have reported on the changes in the microstructure and electric properties of ITO films with respect to the film thickness (Ref 38).

In this case, the films have been deposited using the SPT which is somewhat similar to CVD processes and the film morphologies deposited with different substrate temperatures are described. The 2D and 3D AFM micrographs of the ITO samples I_{450}, I_{475}, I_{500}, and I_{525} are shown alternatively in Fig. 7(a and b), (c and d), (e and f), and (g and h), respectively. For I_{450} sample, the distribution of random, diminished spherical grains with some small cracks and voids can be seen over the entire surface. The beginning of grain agglomeration is noticed at some favorable nucleation sites. A nonuniform distribution, with cluster formation (350 nm × 100 nm) in some region can be seen from figure. The surface roughness is quite high. The surface morphology of I_{475} sample deposited at high temperature is improved as compared to I_{450} sample, due to additional sufficient energy required for the decomposition of droplet resulting into crystallites. The randomly oriented, heterogeneous distribution of spherical grains with relatively smooth surface is observed over the film. The distance in between the two small or large grains seems to be clearly darker as compared with the grains. Fine well-growing grains at certain favorable nucleation growth centers of uneven heights are observed from 3D images of I_{475} sample. The morphology of I_{500} sample seems to be more compact with densely packed spherical grains. The inner dark region in between two grains has almost disappeared completely. A nice 3D morphology of same sample suggests that the grains are growing almost all over the films. Homogenous distribution of perfectly cubic grains of 200 nm are seen for I_{500} sample at $1 \times 1\ \mu m^2$ scan (Fig. 8a and b). This temperature seems to be most favorable for grain refining and appropriate for all the nucleation centers present over the entire surface. The heterogeneous distribution of cubic grains with reduced grain density due to higher decomposition temperature is observed for I_{525} sample. The 3D image supports the conclusion. In conclusion, the I_{500} sample has the best morphology. At higher magnification, the grains of I_{500} and I_{525} samples seem to be perfectly cubic, but they differ in grain size. These changes in the morphology are analogues to the improvement in the electrical parameters. The AFM study supports the XRD and SEM studies that the crystallinity increases up to I_{500} sample which thereafter decreases for I_{525} sample. The overall influence of the deposition temperature leads to the ITO films with improved physical properties.

3.5 Electrical Measurements

Figure 9 shows the plot of room temperature (R_T) electrical resistivity for I_{450}, I_{475}, I_{500}, and I_{525} samples. The electrical resistivity (R_T) decreases from 4.27×10^{-3} to $1.96 \times 10^{-3}\ \Omega$ cm for I_{450} to I_{500} samples. The minimum resistivity obtained in this study is comparable to the value reported (Ref 15). The decrease in resistivity with increase in substrate temperature can be explained by the fact that the grain size increases significantly with increase in deposition temperature, reducing grain boundary scattering, and increasing conductivity. The decrease in resistivity can be associated with the observed increase in carrier concentration. For the sample I_{525}, the resistivity increases to $5 \times 10^{-3}\ \Omega$ cm, which may be due the contamination of the samples by alkali ions from the glass substrates (Ref 39) and can be explained by the number of oxygen vacancies in the ITO films.

The conductivity of films is related to the carrier concentration and Hall mobility of films. The conductivity of the samples is 229.8, 342.8, 510.3, and 197.5 Ω for the I_{400} to I_{525} samples. It is well known that the carrier concentration of ITO films is dependent on nonstoichiometry and is also affected by structural defects (Ref 40). The variation of carrier concentration and mobility is shown in Fig. 10. The carrier concentration varies from 0.39 to $3.26 \times 10^{20}\ cm^{-3}$ for the I_{450} to I_{500} samples and then decrease to $0.78 \times 10^{20}\ cm^{-3}$ for I_{525} sample. The mobility of the deposited ITO films varies from 36.78 to 15.81 cm^2/V s. The I_{500} sample exhibits a carrier concentration and mobility of $3.26 \times 10^{20}\ cm^{-3}$ and 9.77 cm^2/V s, respectively.

The mean free path value of carriers (Ref 41) varies over 58-29 nm. The I_{500} sample has minimum free path of 29 nm. Among the different scattering mechanisms, the grain boundary mechanism found to be dominant and can be decided by comparing the mean free path (l) of the carriers (Ref 41) and with crystallite size. If both these values are comparable, then grain boundary scattering mechanism is said to dominant. The mean free path values as indicated above are less than the crystallite dimensions of 45-66 nm, calculated using x-ray data. Since these values are not comparable, grain boundary scattering could be excluded. The mobility decreases with an increase in the carrier concentration, due to the possibility of the ionized impurity scattering. The degeneracy of the samples is confirmed by the evaluation of the Fermi energy level using the relation (Ref 41) from the literature $E_F = \left(\frac{h^2}{8m^*}\right)\left(\frac{3n}{\pi}\right)^{2/3}$, where m^* is the value of effective mass, $0.19me$ (me is the rest mass of electron), and n is the carrier concentration. The Fermi energy values are found to vary over 0.23-0.92 eV, which are higher than the energy corresponding to the room temperature. The straight line nature of the graph of $n^{2/3}$ versus E_F gives direct evidence of degenerate semiconductors. The IR reflectivity of the samples estimated using the equation

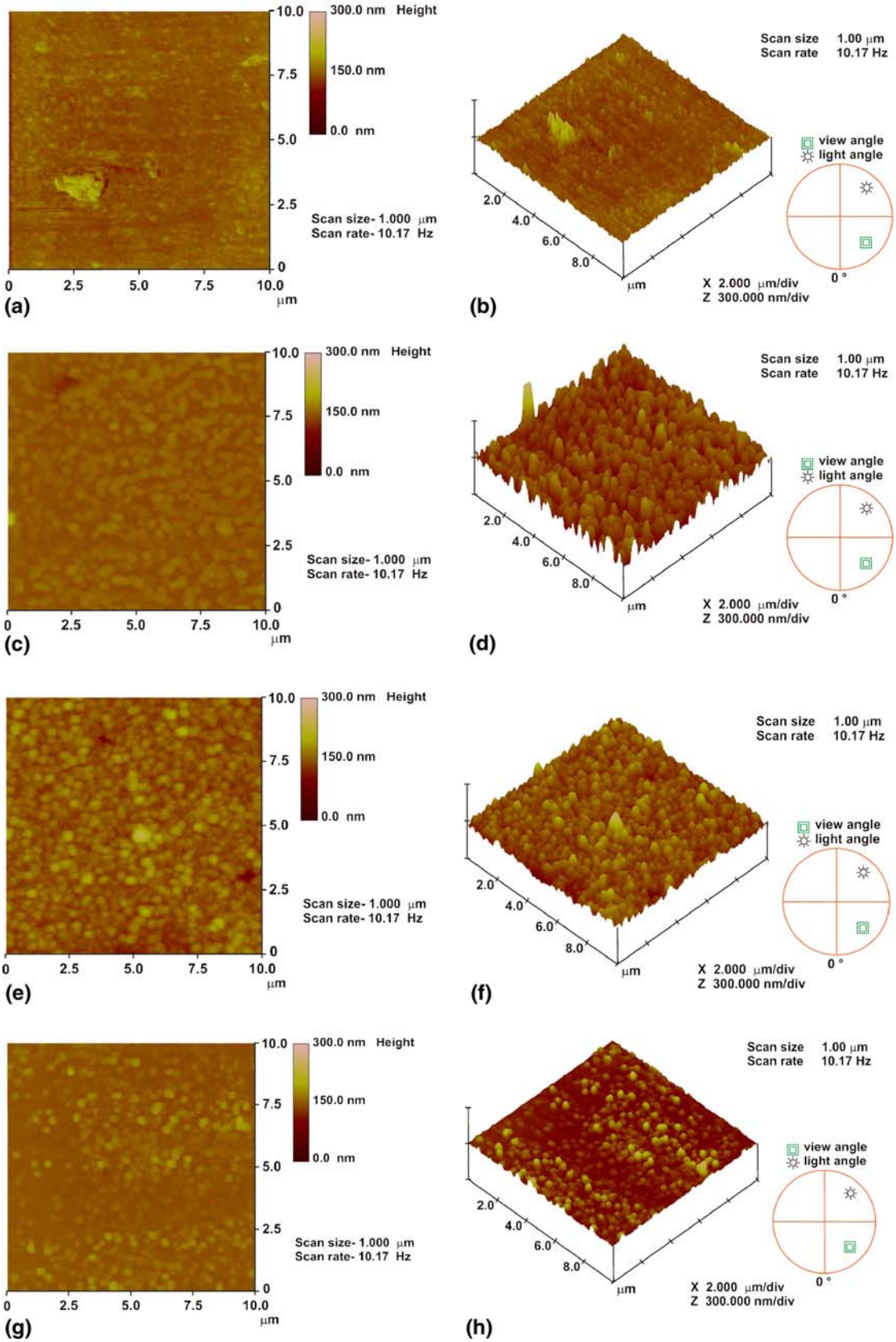

Fig. 7 The 2D and 3D AFM images of ITO films deposited with different substrate temperatures: 450 °C [(a) and (b)], 475 °C [(c) and (d)], 500 °C [(e) and (f)], and 525 °C [(g) and (h)], respectively

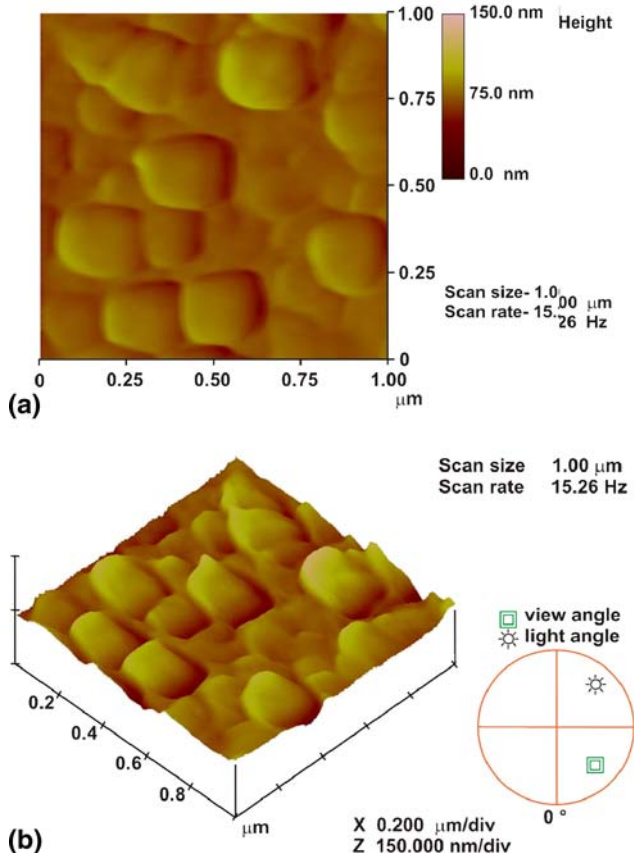

Fig. 8 2D (a) and 3D (b) AFM images of the typical ITO film at 1×1 µm^2 scan

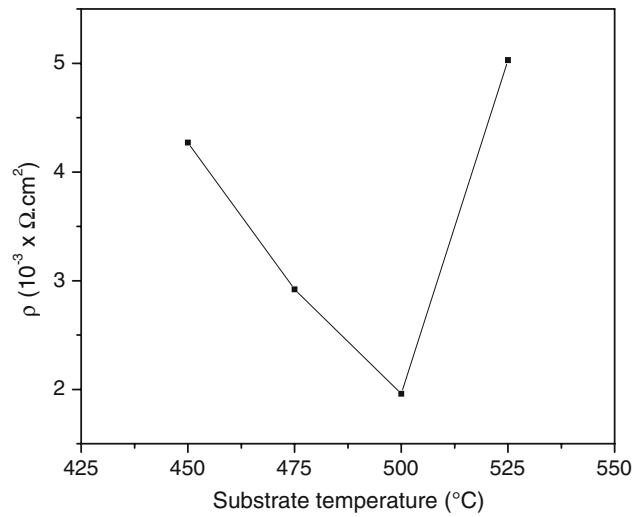

Fig. 9 The variation of resistivity of the ITO film deposited with substrate temperatures

(Ref 42) is found to be in the range of 82-96%. Since IR reflectance of the films is high, they can be used as the different electrode and plate collectors. ITO shows high reflectance in near-infrared zone, which is absolutely

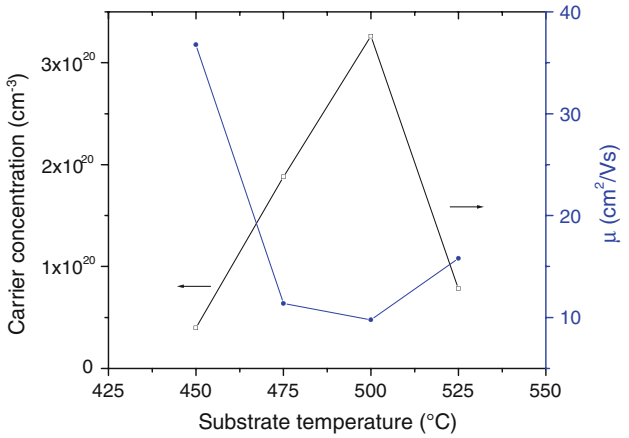

Fig. 10 The variation of carrier concentration and mobility of the ITO film prepared at different substrate temperatures

necessary in solar cell devices, low optical reflectance in the visible region but high in the infrared region. These optical results are in good agreement with literature on ITO (Ref 43). The various structural, optical, electrical, and opto-electrical parameters are tabulated in Table 2. The rough surface decreases carrier mobility, increases light scattering and hence deteriorates the opto-electrical property of display devices and hence surface morphology is one of the most important properties of ITO films for opto-electronic device applications. Similar types of results have been reported by others wherein the surface of ITO is found to be quite rough (Ref 44).

3.6 Figure of Merit

The variation of sheet resistance and the figure of merit is shown in Fig. 11. The decrease in sheet resistance from 97 to 78 Ω/cm^2 for I_{450} to I_{500} samples is attributed to improved crystallinity. The increase in the sheet resistance (129 Ω/cm^2) for I_{525} sample is due to diffusion of mobile alkali metal impurities (like Na^+) from the glass substrate into the ITO films. This effect is particularly noticeable for tin oxide, because sodium diffuses rapidly at the high substrate temperatures. The figure of merit is calculated using the relation $\phi_{TC} = T^{10}/R_s$ from the literature (Ref 45), where R_s is the sheet resistance and T is the transmittance at 550 nm. The I_{500} sample has highest figure of merit value (4.43×10^{-3} Ω^{-1}), which is higher than the values reported (Ref 10, 45) and comparable to 5.4×10^{-3} Ω^{-1} (Ref 46).

4. Conclusions

The structural, optical, and electrical properties of cost effective sprayed ITO thin films have been found to be influenced by the deposition temperature. The crystalline quality of the films gets better and the grain size increases. During the thermal crystallization process, the resistance decreases and a simultaneous variation in the optical transmission occurs. In particular, resistivity of the film

Table 2 The different parameters estimated from optical absorption and Hall Effect measurements for ITO films deposited at different substrate temperatures

Temperature, °C	R_s, Ω/cm^2	t, mm	T, %	ϕ, 10^{-3}, Ω^{-1}	ρ, 10^{-3}, Ω cm	n, 10^{20}, cm^{-3}	μ, cm^2/V s	E_F, eV	l, nm	E_g, eV	D, nm
450	97.1	250	81.5	1.18	4.27	0.39	36.78	0.23	58.62	3.56	45
475	89.7	325	82.6	1.69	2.92	1.88	11.38	0.64	34.90	3.6	58
500	78.3	440	84.3	4.43	1.96	3.26	9.77	0.92	29.05	3.72	66
525	129.1	390	83.1	1.26	5.03	0.78	15.81	0.36	46.72	3.74	62

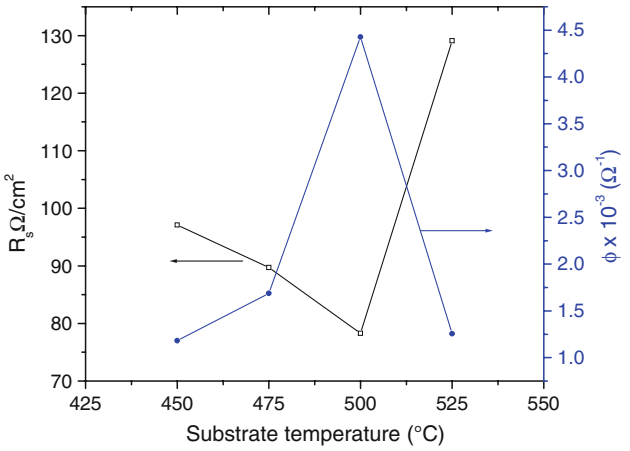

Fig. 11 The plot of sheet resistance and the figure of merit of the ITO film as function of substrate temperatures

decreases to a minimum of 1.96×10^{-3} Ω cm. The SEM and AFM study shows that the deposition temperature influences the morphology of the ITO samples. The well-grown, cubic grains are observed for I_{500} sample, with maximum carrier concentration of 3.26×10^{20} cm^{-3} and mobility of 9.8 cm^2/V s. The highest figure of merit value is 4.43×10^{-3} Ω^{-1}. The Hall Effect measurements and straight line nature of $n^{2/3}$ versus E_F plot gives direct evidence of degenerate semiconductors. The studied samples have IR reflectance and therefore can be used in different photo-electrode applications.

Acknowledgments

A.V. Moholkar is grateful to the Department of Science and Technology, New Delhi for awarding the BOYSCAST Fellowship (File No. SR/BY/P-02/2008) and University Grants Commission, New Delhi, India for the financial assistance through the minor research Projects No. F-47-345/2004 and No F-47-707/2008. P.S. Shinde is highly acknowledged for his efforts in improving the quality of the letters of the AFM images.

References

1. I. Hamberg and C.G. Granqvist, Evaporated Sn-Doped In_2O_3 Films: Basic Optical Properties and Applications to Energy-Efficient Windows, *J. Appl. Phys.*, 1986, **60**(11), p R123-R160
2. K.L. Chopra, S. Major, and D.K. Pandya, Transparent Conductors—A Status Review, *Thin Solid Films*, 1983, **102**, p 1
3. A.L. Dawar and J.C. Joshi, Review Semiconducting Transparent Thin Films: Their Properties and Applications, *J. Mater. Sci.*, 1984, **19**, p 1-23
4. H. Kawazoe, H. Yanagi, K. Ueda, and H. Hosono, Transparent p-Type Conducting Oxides: Design and Fabrication of p-n Heterojunctions, *MRS Bull.*, 2000, **25**(8), p 28-36
5. R.G. Jordan, Criteria for Choosing Transparent Conductors, *MRS Bull.*, 2000, **25**, p 52
6. M. Rottmann, H. Hennig, B. Ziemer, R. Kalähne, and K.H. Heckner, Variations in Microstructure and Composition of Indium Tin Oxide Films with the Deposition Technique, *J. Mater. Sci.*, 1996, **31**(24), p 6495-6500
7. K.R. Subba, V.S. Raja, A.K. Bhatnagar, R.D. Tomlinson, R.D. Pilkington, A.E. Hill, S.J. Chang, and F.S. Juang, Optical, Structural and Electrical Properties of Tin Doped Indium Oxide Thin Films Prepared by Spray-Pyrolysis Technique, *Semicond. Sci. Tech.*, 2000, **15**(7), p 676-683
8. A.V. Moholkar, S.M. Pawar, K.Y. Rajpure, V. Ganesan, and C.H. Bhosale, Effect of Precursor Concentration on the Properties of ITO Thin Films, *J. Alloy Compd.*, 2008, **464**, p 387-392
9. A.V. Moholkar, S.M. Pawar, P.S. Shinde, K.Y. Rajpure, C.H. Bhosale, and J.H. Kim, Physical Properties of Transparent and Conductive Sprayed ITO Thin Films: Optimization of Process Parameters for Highest Figure of Merit Films, 2009, *Curr. Appl. Phys.* (Accepted)
10. M. Nisha, S. Anusha, Aldrin. Antony, R. Manoj, and M.K. Jayaraj, Effect of Substrate Temperature on the Growth of ITO Thin Films, *Appl. Surf. Sci.*, 2005, **252**(5), p 1430-1435
11. A. El Hichou, A. Kachouane, J.L. Bubendorff, M. Addou, J. Ebothe, M. Troyon, and A. Bougrine, Effect of Substrate Temperature on Electrical, Structural, Optical and Cathodoluminescent Properties of In_2O_3-Sn Thin Films Prepared by Spray Pyrolysis, *Thin Solid Films*, 2004, **458**(30), p 263-268
12. B. Ksapabutr, M. Panapoy, K. Choncharoen, S. Wongkasemjit, and E. Traversa, Investigation of Nozzle Shape Effect on $Sm_{0.1}Ce_{0.9}O_{1.95}$ Thin Film Prepared by Electrostatic Spray Deposition, *Thin Solid Films*, 2008, **516**, p 5618-5624
13. M. Girtan and G. Folcher, Structural and Optical Properties of Indium Oxide Thin Films Prepared by an Ultrasonic Spray CVD Process, *Surf. Coat. Tech.*, 2003, **172**(2-3), p 242-250
14. E. Benamar, M. Rami, C. Messaoudi, D. Sayah, and A. Ennaoui, Structural, Optical and Electrical Properties of Indium Tin Oxide Thin Films Prepared by Spray Pyrolysis, *Sol. Energ. Mater. Sol. C*, 1998, **56**(2), p 125-139
15. J.J. Prince, S. Ramamurthy, B. Subramanian, C. Sanjeeviraja, and M. Jayachandran, Spray Pyrolysis Growth and Material Properties of In_2O_3 Films, *J. Cryst. Growth*, 2002, **240**(1-2), p 142-151
16. G. Korotcenkov, V. Brinzari, A. Cerneavschi, A. Cornet, J. Morante, A. Cabot, and J. Arbiol, Crystallographic Characterization of In_2O_3 Films Deposited by Spray Pyrolysis, *Sens. Actuat. B Chem.*, 2002, **84**(1), p 37-42
17. M.J. Alam and D.C. Cameron, Optical and Electrical Properties of Transparent Conductive ITO Thin Films Deposited by Sol-Gel Process, *Thin Solid Films*, 2000, **377-378**, p 455-459
18. P.K. Song, Y. Shigesato, I. Yasui, C.W. Ow-Yang, and D.C. Paine, Study on Crystallinity of Tin-Doped Indium Oxide Films Deposited by DC Magnetron Sputtering, *Jpn. J. Appl. Phys.*, 1998, **37**(4 Suppl A), p 1870-1876
19. V.S. Vaishnav, P.D. Patel, and N.G. Patel, Preparation and Characterization of Indium Tin Oxide Thin Films for Their

Application as Gas Sensors, *Thin Solid Films*, 2005, **487**(1-2), p 277-282
20. D.V. Morgan, Y.H. Aliyu, R.W. Bunce, and A. Salehi, Annealing Effects on Opto-Electronic Properties of Sputtered and Thermally Evaporated Indium-Tin-Oxide Films, *Thin Solid Films*, 1998, **312**(1-2), p 268-272
21. M. Quaas, C. Eggs, and H. Wulff, Structural Studies of ITO Thin Films with the Rietveld Method, *Thin Solid Films*, 1998, **332**(1-2), p 277-281
22. E.J.J. Martin, M. Yan, M. Lane, J. Ireland, C.R. Kannewurf, and R.P.H. Chang, Properties of Multilayer Transparent Conducting Oxide Films, *Thin Solid Films*, 2004, **461**(2), p 309-315
23. A.M.E. Raj, K.C. Lalithamaika, V.S. Vidhya, G. Rajagopal, A. Thayumanavan, M. Jayachandran, and C. Sanjeeviraja, Growth mechanism and Photo-Electronic Properties of Nanocrystalline In_2O_3 Films Prepared by Chemical Spray Pyrolysis of Metal Organic Precursor, *Physica B*, 2008, **403**, p 544-554
24. P.S. Patil, Versatility of Chemical Spray Pyrolysis Technique, *Mater. Chem. Phys.*, 1999, **59**(3), p 185
25. M. Scholten and J.E.A.M. van der Meerakker, On the Mechanism of ITO Etching: The Specificity of Halogen Acids, *J. Electrochem. Soc.*, 1993, **140**(2), p 471-475
26. J.C. Vigue and J. Spitz, Chemical Vapor Deposition at Low Temperatures, *J. Electrochem. Soc.*, 1975, **122**, p 585
27. D. Perednis and L.J. Gauckler, Thin Film Deposition Using Spray Pyrolysis, *J. Electroceram.*, 2005, **14**, p 103-111
28. J.C. Manifacier, M. De Murcia, J.P. Fillard, and E. Vicario, Optical and Electrical Properties of SnO_2 Thin Films in Relation to Their Stoichiometric Deviation and Their Crystalline Structure, *Thin Solid Films*, 1977, **41**(2), p 127-135
29. P. Thilakan and J. Kumar, Oxidation Dependent Crystallization Behavior of IO and ITO Thin Films Deposited by Reactive Thermal Deposition Technique, *Mater. Sci. Eng. B*, 1998, **55**, p 195-200
30. P. Prathap, Y.P.V. Subbaiah, M. Devika, and K.T. Ramakrishna Reddy, Optical Properties of In_2O_3 Films Prepared by Spray Pyrolysis, *Mater. Chem. Phys.*, 2006, **100**, p 375-379
31. E. Burstein, Anamolus Optical Absorption in InSb, *Phys. Rev.*, 1954, **93**, p 632-633
32. M. Kul, M. Zor, A.S. Aybek, S. Irmak, and E. Turan, Electrical and Optical Properties of Fluorine-Doped CdO Films Deposited by Ultrasonic Spray Pyrolysis, *Sol. Energ. Mater. Sol. C*, 2007, **91**, p 882-887
33. P. Debye and P. Scherrer, Interferenzen an Regellos Orientierten Teilchen in Rontgenlight (Interference of Irregularly Oriented Particles in X-rays), *Phys. Zeit.*, 1916, **17**, p 277-283
34. S. Xu and G.Q. Lu, Effect of Atomic Surface Mobility on the Nucleation and Island Growth of Thin Films, *J. Mater. Sci. Lett.*, 1994, **13**, p 1629-1631
35. M. Ohring, *The Materials Science of Thin Films*, Academic Press, San Diego, 1992
36. X.W. Sun, H.C. Huang, and H.S. Kwok, On the Initial Growth of Indium Tin Oxide on Glass, *Appl. Phys. Lett.*, 1996, **68**, p 2663
37. Y. Sato, M. Taketomo, N. Ito, and Y. Shigesato, Study on Early Stages of Film Growth for Sn Doped In_2O_3 Films Deposited at Various Substrate Temperatures, *Thin Solid Films*, 2008, **516**, p 5868-5871
38. D.H. Kim, M.R. Park, H.J. Lee, and G.H. Lee, Thickness Dependence of Electrical Properties of ITO Film Deposited on a Plastic Substrate by RF Magnetron Sputtering, *Appl. Surf. Sci.*, 2006, **253**, p 409-411
39. H. Kim, J.S. Horwitz, W.H. Kim, Z.H. Kafafi, and D.B. Chrisey, Highly Oriented Indium Tin Oxide Films for High Efficiency Organic Light-Emitting Diodes, *J. Appl. Phys.*, 2002, **91**, p 5371
40. J.S. Cho, K.H. Yoon, and S.K. Koh, Microstructure of Indium Oxide Films in Oxygen Ion-Assisted Deposition, *Thin Solid Films*, 2000, **368**(1), p 111-115
41. B. Thangaraju, Structural and Electrical Studies on Highly Conducting Spray Deposited Fluorine and Antimony Doped SnO_2 Thin Films from $SnCl_2$ Precursor, *Thin Solid Films*, 2002, **402**(1-2), p 71-78
42. G. Frank, E. Kauer, and H. Köstlin, Transparent Heat-Reflecting Coatings Based on Highly Doped Semiconductors, *Thin Solid Films*, 1981, **77**(1-3), p 107-118
43. H. Bisht, H.-T. Eun, A. Mehrtens, and M.A. Aegerter, Comparison of Spray Pyrolyzed FTO, ATO and ITO Coatings for Flat and Bent Glass Substrates, *Thin Solid Films*, 1999, **351**, p 109-114
44. J. Zhang, J.Q. Hu, F.R. Zhu, H. Gong, and S.J. Oshea, ITO Thin Films Coated Quartz Crystal Microbalance as Gas Sensor for NO Detection, *Sens. Actuat. B Chem.*, 2002, **87**(1), p 159-167
45. G. Haacke, New Figure of Merit for Transparent Conductors, *J. Appl. Phys.*, 1976, **47**(9), p 4086-4089
46. S.M. Rozati and T. Ganj, Transparent Conductive Sn-Doped Indium Oxide Thin Films Deposited by Spray Pyrolysis Technique, *Renew. Energ.*, 2004, **29**(10), p 1671-1676